Check for
updates

Occurrence Apparent Velocities for Identification and Quantification of Space–Time Clustering Precursory to a Large Earthquake. Application to Large (M > 7.0) Earthquakes in Southern California and Northern Baja California

F. Nava[1] · **H. Reynoso[1]** · **E. Glowacka[1]**

Abstract

Space–time seismic clusters, localized bursts of seismic activity, are a feature of background seismicity before the occurrence of large earthquakes, a feature that agrees with observations of diminishing Gutenberg–Richter b-value, fractal dimension, and entropy, and is therefore suggestive of high stress. However, identification and quantification of these space–time clusters, particularly when they are small, is not an easy task and requires a priori assumptions. A novel method for space–time cluster identification, based on an extension of the concept of apparent velocities, is proposed because space–time clusters in the background seismicity have a particular signature in the apparent velocity domain. The contents of histogram peaks due to clusters in the apparent velocity histogram can be used to quantify the cluster activity compared with null hypothesis levels. Identification of the earthquakes corresponding to the apparent velocities in the peaks allows identification of cluster activity in time and space. Apparent velocity peaks do appear in real catalog data for southern California and northern Baja California before the Landers 1992 $M = 7.3$, Hector Mine 1999 $M = 7.1$, El Mayor-Cucapah 2010 $M = 7.2$, and Ridgecrest 2019 $M = 7.1$ earthquakes, and they appear only within 15 to 25 years before the occurrence of large earthquakes. They are not observed either long before the large earthquakes or after them, and hence could be related to high local states of stress and be of value as a possible precursory observable.

Keywords Seismic clusters · Apparent velocities · Precursors · Statistical seismology

---

✉ F. Nava
fnava@cicese.mx

[1] Seismology Department, CICESE, Carretera Ensenada-Tijuana 3918, Zona Playitas, 22860 Ensenada, B.C, Mexico

🖄 Springer

1 Introduction

Phenomena that occur before large earthquakes, commonly known as precursors, are an important tool for seismic hazard estimation (Rikitake 1976; Evison 1999; Cicerone et al. 2009) and are useful in narrowing the forecast time estimates. Many kinds of precursors have been proposed—electromagnetic, chemical, geodetic, animal behavior, and, of course, seismic—but most of the proposed precursors are not sufficiently well documented, so it is impossible to assess their usefulness and reliability (Wyss 1991, 1997; Zechar and Zhuang 2010). Precursors are assumed to reflect, in different ways, a state of high stress in a given region.

To date there is not a single instance of a perfect precursor, that is, one that occurs if and only if there will be a large earthquake in the study region. Hence, it seems reasonable to combine information from several precursors that measure different aspects or characteristics of the seismic process (Aki 1981; Anderson 1982). In consequence, it is important to identify and document possible precursors that can contribute to reliable forecasts.

Among the seismic precursors that have been proposed are changes in the seismicity rate and/or location, including increased seismicity, quiescence, and doughnut patterns (Kanamori 1981; Chen et al. 1999; McGuire et al. 2005; Mignan 2014; Adamaki and Roberts 2017), changes in the Gutenberg–Richter b-value (Smith 1986; Enescu and Ito 2001; Wang et al. 2016), changes in the fractal dimensions of the spatial distribution of seismicity (Goltz 1997; Enescu and Ito 2001; Márquez et al. 2012; Michas et al. 2015), and changes in other properties of the seismicity.

One seismic precursor that has been observed is clustering in the background seismicity, but the term earthquake, or seismic, cluster is used to mean different things: catalogs are "declustered" to eliminate aftershocks (Zaliapin et al. 2008); epicentral distributions that depart from usual distributions, such as doughnut patterns or foreshocks, are said to be clustered (Ogata et al.1995); Rikitake (1976) uses the term to denote some kind of seismic station; many studies consider clusters as epi- or hypocentral groupings in space only (Frohlich and Davis 1990; Ester et al. 1996; Lippiello et al. 2012; Czecze and Bondár 2019), while others also take into account the duration of spatial clustering (Telesca et al. 2001; Vidale and Shearer 2006; Yang et al. 2009; Hall et al. 2018). Zaliapin and Ben-Zion (2013) state that there is no formal definition of a cluster, yet the same authors (Zaliapin and Ben-Zion 2016) define clustering as a partitioning of seismicity into groups closer in space and time than expected in a purely random distribution. This last definition of cluster is very much like the simplified one that will be used in this paper.

Since clustering in this later sense seems to occur in conditions of high ambient stress (Hall et al. 2018), as indicated by coincident diminutions in b-value, fractal dimension, and entropy (Geilikman et al. 1990; Dimitriu et al. 2000; Main and Al-Kindi 2002, Márquez-Ramírez et al. 2012; Nanjo et al. 2012; Nava et al. 2021), identification and characterization of seismic clusters is an important task.

However, most cluster identification methods are quite complicated and involve a large number of a priori assumptions and parameters that have to be adjusted (Frohlich and Davis 1990; Ester et al. 1996; Weatherill & Burton 2009; Rehman et al. 2014; Hall et al. 2018; Czecze and Bondár 2019; Yang et al. 2019). The present paper proposes a

completely different and novel approach to cluster identification and characterization, based on a generalization of the concept of apparent velocity, that involves a minimum of assumptions and only two non-critical parameters. The method is justified by its results when applied to real data.

2 Apparent Velocities

The traditional concept of apparent velocity corresponds to the observation of the arrival of a seismic wavefront at different stations, as illustrated in Fig. 1, where triangles represent seismic stations. The red line is a wavefront traveling with speed β in the direction of the arrow, r is the distance between the stations, and t_1 and t_2 are the arrival times at the first and the second station, respectively. Let $\tau = t_2 - t_1$, and let the measured velocity be $v = r/\tau$ (it should properly be called "speed" but is customarily called "velocity"). When the wavefront travels parallel to the line between the stations (Fig. 1A) $\tau = r/\beta$ and the measured velocity equals β, but when the wavefront forms an angle γ with the line (Fig. 1B), then $\tau = d/\beta = r \cos \gamma /\beta$ and becomes smaller as γ grows, so that for $\gamma = 90°$, $\tau = 0$ and $v = \infty$. This measured velocity, ranging from β to ∞, although having velocity (space/time) units, does not involve transmission of mass or energy from one station to the other, so it is not a true velocity between stations. It is an apparent velocity.

Let us extend the concept of apparent velocities to apparent occurrence velocities. Consider an ordered set of earthquakes $e_i = (t_i, x_i, y_i, z_i, M_i)$; $i = 1, \cdots, N$, with times $t_i \leq t_j$ for $i < j$, coordinates x_i, y_i, z_i (in km), and magnitudes M_i, occurring within a volume with limits $[x_{min}, x_{max}]$, $[y_{min}, y_{max}]$, and $[z_{min}, z_{max}]$, during a time interval $[t_1, t_N]$. Let the difference in times between the occurrence of events i and j
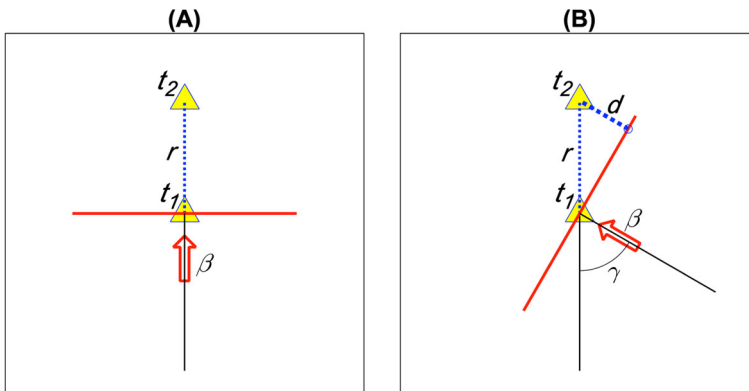
Fig. 1 Apparent velocity. Triangles are seismic stations separated by a distance r, reached by a wavefront, indicated by the thick red line, traveling with speed β in the direction indicated by the arrow, at times t_1 and t_2. The angle between the wavefront direction and the line between the stations is 0 in (**A**) and γ in (**B**)

be

$$\tau_{ij} = t_j - t_i, \tag{1}$$

and let the distance between their hypocenters be

$$r_{ij} = \sqrt{\left(x_j - x_i\right)^2 + \left(y_j - y_i\right)^2 + \left(z_j - z_i\right)^2}; \tag{2}$$

then, the apparent occurrence velocity (henceforth simply called apparent velocity or AV) is

$$v_{ij} = \frac{r_{ij}}{\tau_{ij}}. \tag{3}$$

Only velocities v_{ij} with $i < j$ will be considered, because $v_{ii} = 0/0$ and $v_{ji} = -v_{ij}$, so velocities for $j \leq i$ do not contain further information. Thus, $N_p = N(N-1)/2$ velocities, each corresponding to a pair of events, will be considered. AVs can take values ranging from zero, for events occurring at the same place at different times, to infinity, for events occurring at different places at the same time.

3 Clusters

A simplified definition of cluster, very much like the one in Zaliapin and Ben-Zion (2016), will be used for the cluster identification approach presented in this paper; the definition serves to identify the object of study and to model what would be expected from the AV study, but it sets no hard conditions on the data.

A seismicity space–time cluster, hereafter called simply cluster, is defined as a localized burst of seismicity, which means many earthquakes within a small volume and a short interval. Many, small, and short are not precise terms, and in some studies their values have to be defined a priori, but in the AV approach, their values result naturally from the study.

To form an idea of what can be expected from apparent velocities, a cluster can be roughly modeled as a group of N_1 earthquakes with hypocenters uniformly distributed within a spherical volume with radius ρ and origin times distributed over a period of length 2θ, as illustrated in Fig. 2; the cosine time distribution was chosen to mimic activity starting and ending gradually. Of course, real clusters may have spatial and temporal distributions that differ from those of this model, but, as will be shown when considering real data, the actual distributions in real clusters do not change the main features of the AVs, so the proposed model does appropriately illustrate the main features of real cluster activity.

First, consider the AVs corresponding to ordered pairs of events all belonging to a given cluster, i.e., intra-cluster AVs. Figure 3 shows a synthetic space–time cluster and the corresponding r, τ, and v distributions. This cluster has $N_1 = 100$ hypocenters distributed uniformly within a sphere with radius $\rho = 1$ km and times cosine-distributed with $\theta = 0.1$ year. The r values range from 0 to 2ρ, but most have values in the $\approx 0.4\rho$

Fig. 2 Model of a space–time cluster: uniform spatial distribution within a spherical volume with radius ρ (top), and cosine temporal distribution over a 2θ interval (bottom)
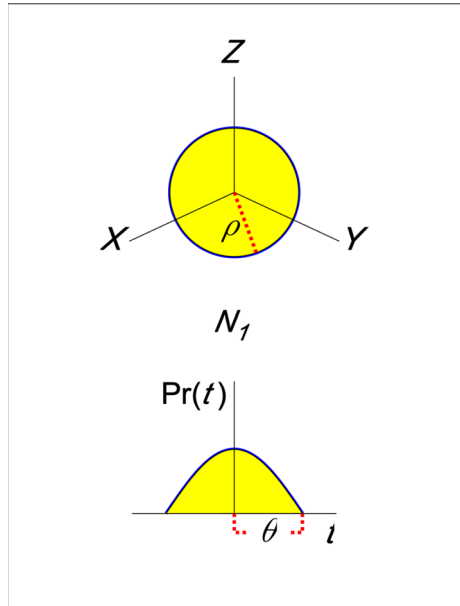
to $\approx 0.8\rho$ range, while small τ values are the most numerous over the 0 to 2θ range. While velocities do have a wide range (this particular example had a maximum velocity of 55,858.09 km/year), most of the intra-cluster $N_{p1} = N_1(N_1 - 1)/2$ velocities fall within the range shown in Fig. 3 (bottom), with an unimodal distribution typically having its mode around $v \sim 0.8\rho/\theta$ km/year in a peak that is quite narrow compared to the possible infinite range of the velocities. This narrow, low-velocity peak in the intra-cluster AV histogram, containing most of the N_{p1} velocities, is typical of all clusters modeled or observed so far, which means that clusters have a particular signature in the AV histogram.

The units for all histograms shown in this paper are counts normalized by the total number of velocities, and will be referred to as normalized counts (NCs), and the histograms will be labeled as H.

In practice, clusters are never isolated, because a state of high stress is conducive to having all types of seismicity. Thus, the next step is to consider AVs between events in a cluster and an event outside it, as schematized in Fig. 4A, where the cluster is represented as a sphere and the external event as an asterisk.

The distance between the outside event and the center of the cluster is R, and the time between the origin time of the external event and the middle time of the cluster is T; hence, if the cluster has N_1 events, for each external event there will be N_1 AVs ranging from $V_{\min}$ to $V_{\max}$, where

$$V_{\min} = \frac{R - \rho}{T + \theta}, \quad V_{\max} = \frac{R + \rho}{T - \theta}. \tag{4}$$
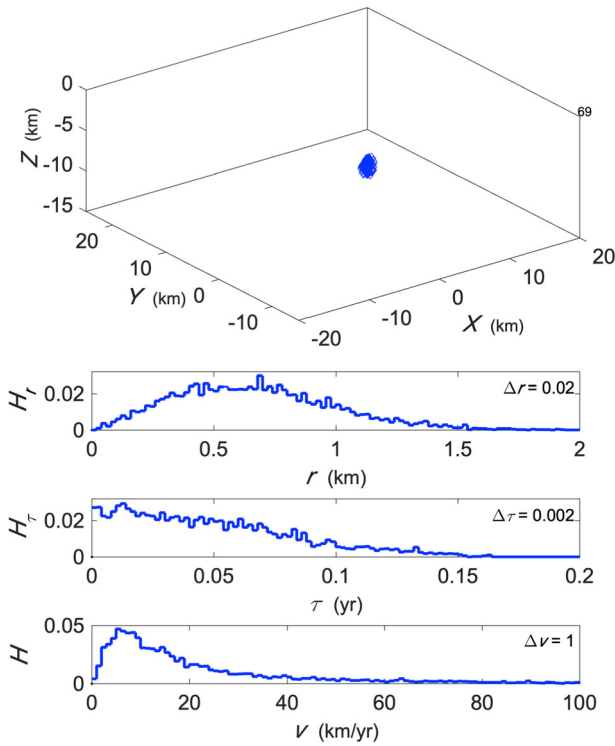
Fig. 3 A single cluster (top) and its corresponding r, τ, and v distributions, indicated by H_r, H_τ, and H, respectively; Δr, $\Delta \tau$, and Δv are the class widths (in the appropriate units), and the total number of velocities in this example is N_{p1}
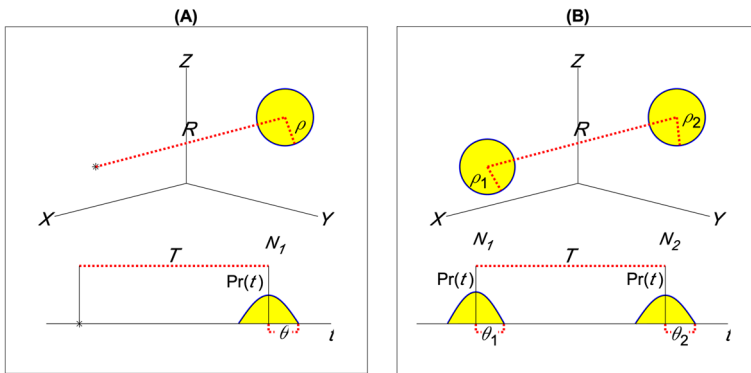
Fig. 4 A A single external event and a cluster. **B** Two clusters, in both space (top) and time (bottom)

In high-stress regimes it is not uncommon to have more than one cluster in a given seismicity sample. For an approximate estimate of the AVs that can be expected from a pair of clusters, let the clusters be represented as spheres (Fig. 4B, top) with radii ρ_1 and ρ_2, and let the distance between the centers of the spheres be R. Now let the occurrence times of events in each cluster be cosine-distributed around a central value, within bands $2\theta_1$ and $2\theta_2$ wide, and let the time between the central times of the clusters be T (Fig. 4B, bottom). Now, the distances between hypocenters and the intervals between occurrence times of pairs of events, each event in a pair belonging to a different cluster, will be within small ranges.

The AVs for events located at the center of the clusters and occurring in the middle of the time ranges will be

$$V = R/T, \tag{5}$$

and, if the clusters have N_1 and N_2 events, respectively, they will result in $N_{p12} = N_1 N_2$ apparent AVs that will range from $V_{\min}$ to $V_{\max}$, where

$$V_{\min} = \frac{R - \rho_1 - \rho_2}{T + \theta_1 + \theta_2}, \quad V_{\max} = \frac{R + \rho_1 + \rho_2}{T - \theta_1 - \theta_2}. \tag{6}$$

When R and T are large with respect to ρ and θ, respectively, the inter-cluster AVs of these pairs will be within a small range and will appear as a narrow peak in the AV histogram. However, when T is not large with respect to θ, the denominator in $V_{\max}$ can become very small or zero, and the apparent velocities will have a large spread and consequently the histogram peak will have small amplitude.

In order to visualize how realistic seismicity would appear in the AV analysis and how this analysis is carried out, a synthetic realization involving three clusters, seismicity distributed uniformly along a band (such as seismicity from a fault system), and completely random uniformly volume-distributed events is presented (Fig. 5). The clusters are numbered sequentially: cluster 2 occurs 2 years after cluster 1, and cluster 3 occurs 2.5 years after cluster 2; they have 70, 60, and 65 events, respectively. The r distribution shows four peaks: one around 0.5 km corresponding to all the intra-cluster distances, and three each corresponding to a cluster pair. Time differences show smoother peaks, with small intra-cluster differences and overlapping ones for two cluster pairs. AVs show two main peaks, one corresponding to those from the 1–3 cluster pair, and, as will be shown later, most of the intra-cluster velocities. Another smaller and wider peak contains velocities from the 1–2 and 2–3 cluster pairs. It should be mentioned that the largest AV was 609,038 km/year but, as can be seen in the plot, the number of velocities in each $\Delta v = 0.1$ km/year class is negligible above 15 to 20 km/year, so the part of the histogram above these velocities will not be shown.
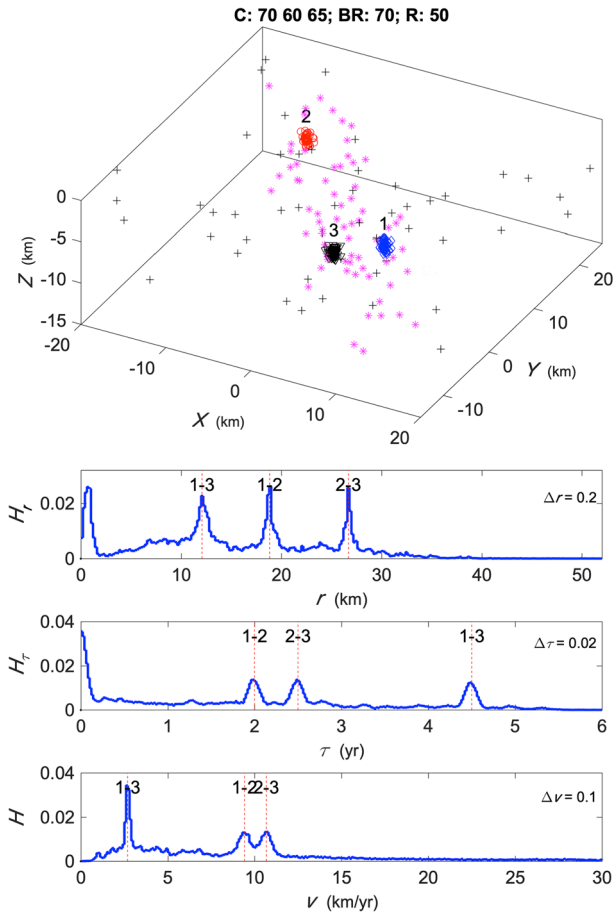
Fig. 5 Hypocentral distribution of three clusters, plus banded (asterisks) and whole-volume uniformly distributed events (crosses) (top); r, τ, and v distributions, indicated by H_r, H_τ, and H, respectively; Δr, $\Delta \tau$, and Δv are the class widths (in the appropriate units), and the total number of velocities in this example is N_p. Dashed vertical lines indicate R, T, and V for each pair of clusters identified by numbers on each side. In the title, C indicates the number of events in each cluster, BR is the number of events distributed randomly with uniform probability within a band, and R is the number of events distributed randomly with uniform probability over the whole space

4 The Apparent Velocity Histogram Analysis and Null Hypotheses

The search for space–time clusters in a given region of interest will be done by computing the AVs for events within a chosen time window, building the histogram for a reasonable range of velocities, and looking for significant peaks in it.

Figure 6 (top) shows the result of the AV histogram (AVH) analysis as applied to the synthetic example shown in Fig. 5, as if it were an observed data set, that is, without a priori knowledge of what peaks, if any, are due to. The H distribution shown as a
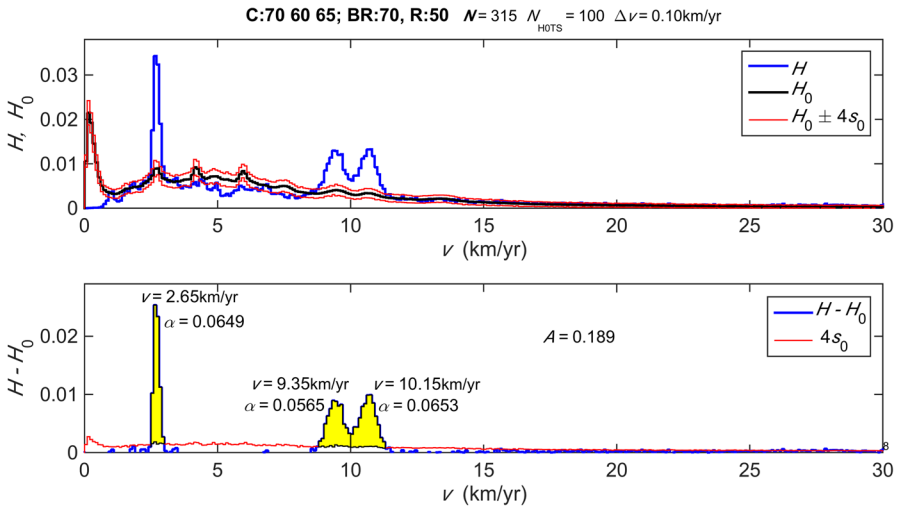
Fig. 6 Top: H and H_0, observed and null hypothesis AV histograms. Bottom: non-negative part of $H - H_0$. Thin lines indicate four null hypothesis standard deviations s_0

thick blue line, is, of course, the same shape as that shown in the bottom picture of Fig. 5.

Significant peaks were mentioned above, so some criterion is needed to decide whether a peak is significant or not; a peak will be considered significant if it has small probability of having occurred by chance. Since peaks are supposed to be due to space–time clustering, it is necessary to see how likely they are to occur when seismicity is not space–time-clustered (the null hypothesis).

The simplest null hypothesis comparison would be to compare the observed (real or synthetic) AV distribution with that resulting from a population having the same number of events distributed uniformly over the same spatial volume and the same time duration as the sample. However, as mentioned above, real seismicity in environments like southern California and northern Baja California (where the method will be applied) is not distributed uniformly in space, but tends to concentrate around faults (Hauksson 2011), so a more realistic null hypothesis would be to consider the same spatial distribution as the observed one and generate random uniformly distributed times. A more stringent test is to keep the observed hypocenters and the observed times, but shuffle (randomly redistribute) the times among the events. In this null hypothesis scheme, H0TS, the distributions of r_{ij} and τ_{ij} remain the same, but the coincidences among distances and times have been changed. Since the H0TS null hypothesis is the most stringent and realistic, it is the one that will be used as a reference level in what follows.

H_0, the mean of the 100 histograms from Monte Carlo realizations of H0TS catalogs derived from the observed one, is shown in Fig. 6 (top) as a thick (black) line. The figure also shows, as thin red lines, $H_0 \pm 4s_0$, where s_0 is the standard deviation for each H_0 value.

Observed AVs with NCs above $H_0 + 4s_0$ will be considered significant because, according to the Chebyshev inequality (Parzen 1960), they have very small probabilities ≤ 0.03125 of having occurred by chance from a population that is not space–time-clustered. The measure of the total amount of nonrandom space–time clustering of the H distribution is the total number of NCs above $H_0 + 4s_0$, denoted by A, while α denotes the number of NCs above $H_0 + 4s_0$ for individual peaks.

In order to make the relation between H and H_0 easier to see, the non-negative part of $H - H_0$ is plotted in Fig. 6 (bottom) together with the $4s_0$ curve; the areas above $4s_0$ have been shaded in the figure. It is in this plot that significant peaks are identified; a given peak spans from v_1 to v_2, which are the first and last velocities to have histogram values above the $4s_0$ level on each side of the velocity corresponding to the highest $H - H_0$ value in the histogram peak.

To give an idea of the relative sizes of the α and A quantities, from the total unit area of each H and H_0, in the velocity range $v \leq 30$ km/year shown in Fig. 6, the total NC of H is 0.8579 and that of H_0 is 0.7883; the total NC of H above H_0 is 0.2691, and that above $H_0 + 4s_0$ is 0.1886.

This AV identification and evaluation of space–time clustering in background seismicity is easily implemented for routine monitoring and, as will be shown in the application, can be used for identification of precursory activity. Before proceeding to the application, it will be shown how AVs can yield other information about the location and times of space–time clustering.

5 The Apparent Velocity Matrix Temporal and Spatial Analysis

The next step in the analysis is to try to determine what events cause the observed velocity histogram peaks.

After selecting a NC peak and its corresponding velocity range above $H_0 + 4s_0$, velocities within the $v_1 \leq v_{ij} \leq v_2$ range are plotted as a color-coded symbol in $t_i \otimes t_j$ space, in what will be called an AV time picture (AVTP), as exemplified in Fig. 7 for the highest peak of Fig. 6. AVs in the chosen range are usually distributed over the entire space, but those associated with space–time clusters appear as groups where velocities diminish from upper left to bottom right. Groups at the diagonal are due to intra-cluster velocities, while other groups are due to inter-cluster velocities or to cluster-individual event velocities. For this example, only two groups will be studied: the group identified by number 1 corresponding to inter-cluster AVs between elements of clusters 1 and 3, and group 2 that is due to intra-cluster velocities from cluster 2. Colored alignments represent velocities between a cluster and individual non-clustered events.

Once groups have been identified in the AVTP (Fig. 7), starting and ending times for each cluster can be read directly from the figure, and it is easy to identify the events contributing to the group; if these are plotted in space, spatial features (if any) related to cluster activity can be identified. Figure 8 shows the events identified as contributing to the two groups in Fig. 7, the earlier events of each pair are shown as triangles and later events are shown as circles.
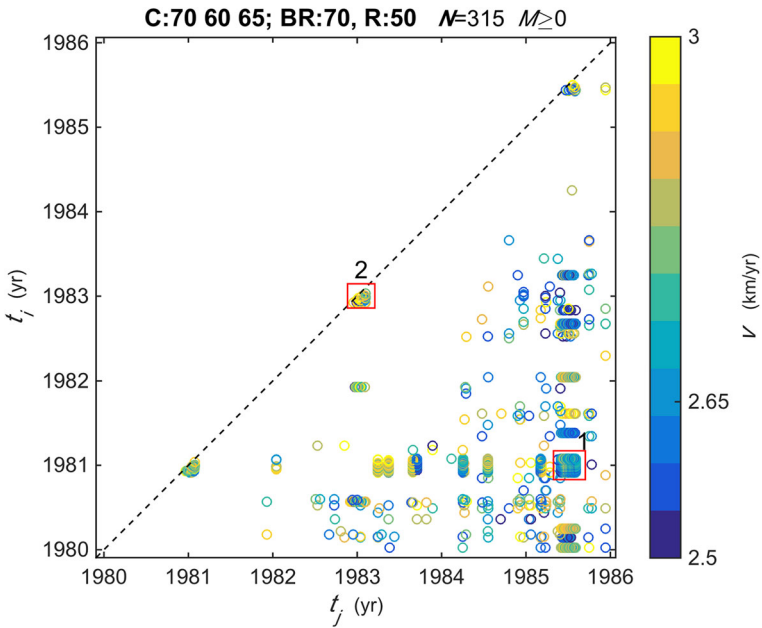
Fig. 7 AVTP: AVs in the $v_1 = 2.50$ km/year to $v_{12} = 3.00$ km/year range in $t_i \otimes t_j$ space, colored according to the velocity color code at right. Selected groups are shown as squares with an identification number on top
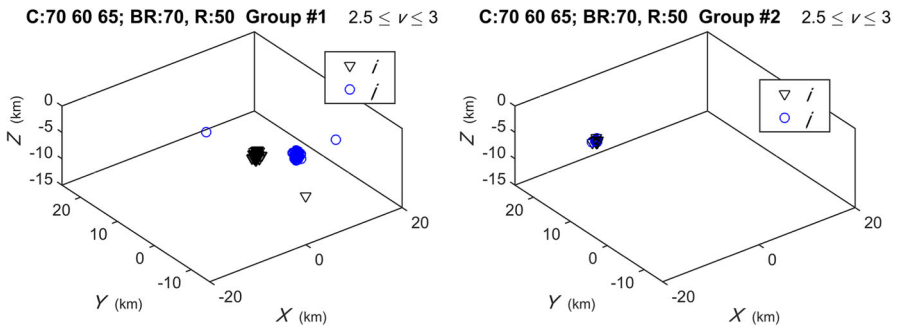
Fig. 8 Spatial location of events contributing to the AVTP groups 1 (inter-cluster, left) and 2 (intra-cluster, right)

The AVTP analysis of the other peaks in Fig. 6 will not be shown here, but it presents two easily identifiable inter-cluster groups.

6 Application to Real Seismicity Data

Having explained the proposed methods of AV identification of space–time clusters and of AVTP analysis, examples of application to real seismicity and to precursory behavior identification will be shown. It should be pointed out that the analyses that follow do not depend at all on the models shown before, which were for illustration only; the results will be due only to the natural AV distributions in the real data. Only two parameters will be used to conduct the analysis, the minimum threshold magnitude and the time window length, and neither of these is critical, since changing them does not give very different results. A reference value of $H_0 + 4s_0$ is used, but any other reference value may be substituted.

In order to test whether real seismicity features peaks in the AV histogram that could be related to the future occurrence of large earthquakes, four large ($M > 7.0$) earthquakes that occurred in southern California and northern Baja California from 1981 to 2019 between longitudes 118.0°W and 114.8°W and latitudes 32.00°N and 36.0°N were studied: Landers 1992 M7.3 (L73), El Mayor-Cucapah 2010 M7.2 (EMC72), Hector Mine 1999 M7.1 (HM71), and Ridgecrest 2019 M7.1 (R71). Only a sample analysis for the largest event, L73, and overall results for all earthquakes will be presented here.

The data are hypocenters from the Southern California Seismic Network (SCSN) catalog. Figure 9 shows the epicenters of events $M \geq 2.5$ that occurred in southern California and northern Baja California within the abovementioned space and time windows; the stars indicate the epicenters of the four largest earthquakes in the period.

The epicenters of seismicity associated with these four major events appear to be distributed in elongated groups or patches, and the proposed velocity determination scheme was applied to hypocenters belonging to the groups that include the major events. The seismicity was separated into time windows to test whether identifiable velocity peaks were present all the time or appeared only before large earthquakes.

All four major earthquakes have been studied extensively elsewhere, so their characteristics, effects, or tectonics will not be discussed here; suffice it to say that all were predominantly strike-slip events, and that their respective epicentral groups appear to be separate from neighboring activity.

6.1 Landers 1992 $M = 7.3$ Earthquake

The largest earthquake in the catalog is the Landers 1992 $M = 7.3$ (L73) event, occurring on May 28, 1992 (1992.4904325) at longitude 116.4315°W, latitude 34.2032°N, and depth $D = 2.79$ km (Figs. 9 and 10). Figure 10 (top) shows epicenters of events occurring before the April 23, 1992, $M = 6.1$ Joshua Tree earthquake, and belonging to the L73 patch which has a narrow, somewhat S-shaped spatial distribution. The L73 epicenter is shown as a yellow star, and the yellow diamond is the epicenter of the Joshua Tree earthquake.

To see whether the AV distribution varied through time, the seismicity was separated into time windows, shown in Fig. 10 together with the cumulative number of events (bottom). Window length has to be a tradeoff between good temporal definition and
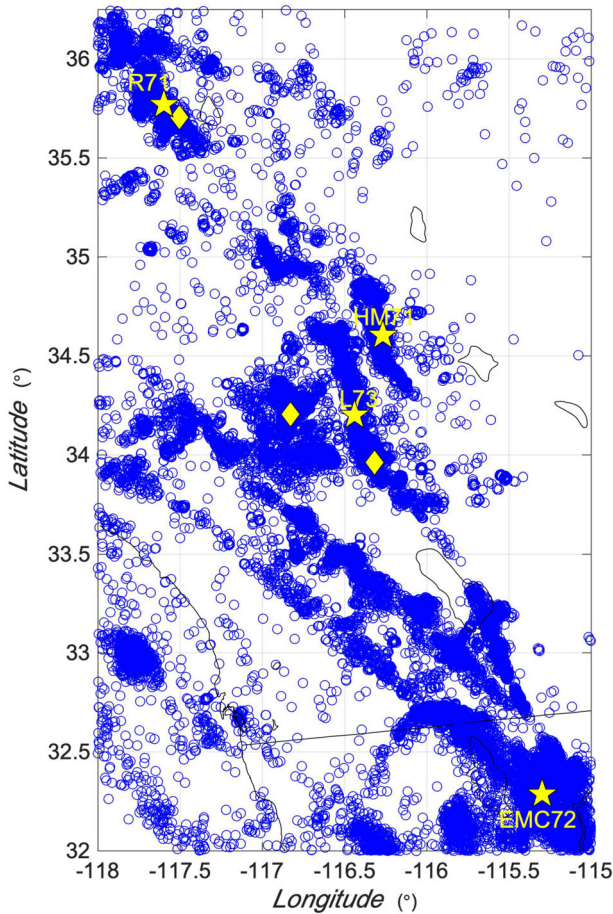
Fig. 9 Epicenters in southern California and northern Baja California from the SCSN catalog. Stars indicate earthquakes with $M \geq 7.0$, with symbol sizes proportional to their magnitudes: L73 is the Landers M7.3 earthquake, EMC72 is the El Mayor-Cucapah M7.2 earthquake, HM71 is the Hector Mine M7.1 earthquake, and R71 is the Ridgecrest M7.1 earthquake. A diamond SSE of L73 is the M6.1 Joshua Tree earthquake, and the diamond west of L73 is the M6.5 Big Bear earthquake. The diamond SE of R71 is the July 4, 2019, Searles Valley $M_W = 6.4$ earthquake. Thin lines indicate the coastline and the Mexico–USA border

having a span long enough to contain clusters well separated in time to give good inter-cluster AV peaks (if there are any clusters); after several trials, 4 years was chosen as a convenient window length.

Time windows are related to the main event occurrence time. The first of the ten windows prior to L73 was set to end in 1992.30 (April 20, 1992) just before the Joshua Tree event, so that it did not include either the M6.1 Joshua Tree earthquake or its aftershocks, because if there had been monitoring before this earthquake, only data before these events would have been used. Any anomalous activity may be considered to have been a precursor to both the Landers and the Joshua Tree earthquakes.
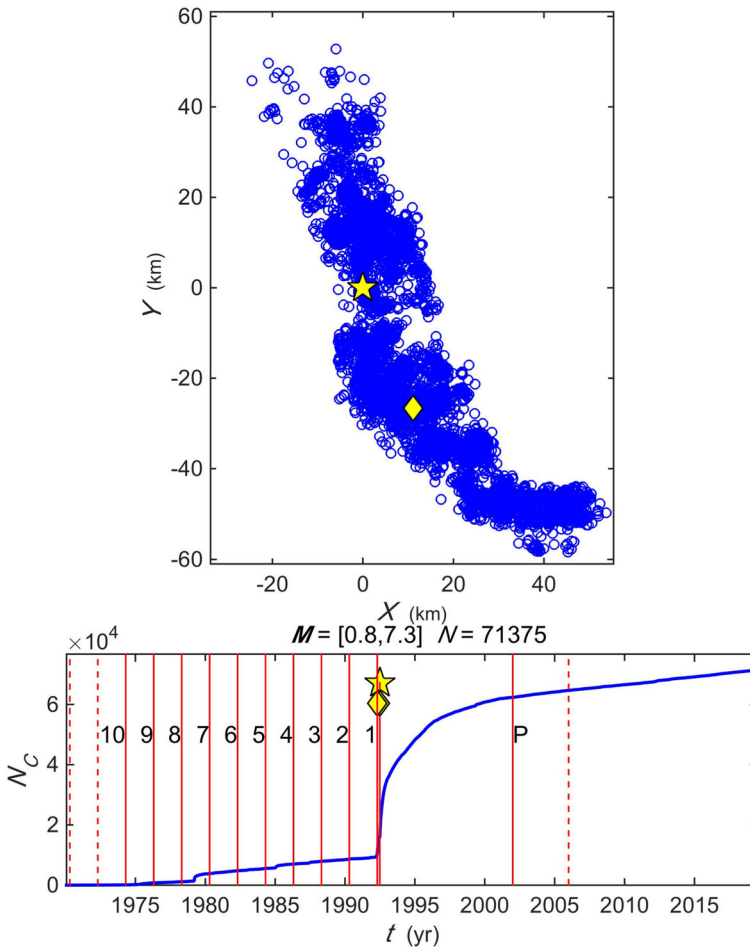
Fig. 10 (Top) Epicenter groups before the L73 earthquake; L73 is indicated by a star and the Joshua Tree earthquake is shown as a yellow diamond. (Bottom) Cumulative number of earthquakes, N_c, as a function of time shown as a thick blue line (bottom). For windows before L73, vertical lines indicate the ending of each time window, and vertical dashed lines indicate the corresponding beginnings; the number or letter at the end of each window is its identification in the text that follows. Window P begins after activity has returned to background level and extends forward in time

The ending time of each consecutive window is shifted by $\Delta t = -2$ years from that of the previous one, and each widow extends backwards in time for 4 years; thus, time windows overlap by 2 years, so that clusters occurring within 2 years are not artificially separated. Windows will be identified as L73 dash the window number shown in Fig. 10. Another window, labeled P in Fig. 10, was chosen in order to sample the seismicity after the main event and after most of the aftershock activity has occurred and stress is expected to be low.

Results will be shown starting with the third window, L73-3, because it contains the largest signal and will be the reference for judging the results from other windows.

For reasons of space, full details of the analysis will be shown only for the sample window.

7 Window L73 -3

Window 3 before L73 spans 4 years, from 1984.309 to 1988.3092, and includes $N = 497$ events with $M \geq 2.2$ shown in Fig. 11 together with the r and τ distributions.

The AVH is shown in Fig. 12 together with H_0 and $H_0 \pm 4s_0$ (top), and $H - H_0$ together with $4s_0$ (bottom). In this last plot seven peaks reach above the $4s_0$ level, and the three largest ones have been shadowed and the corresponding velocities and
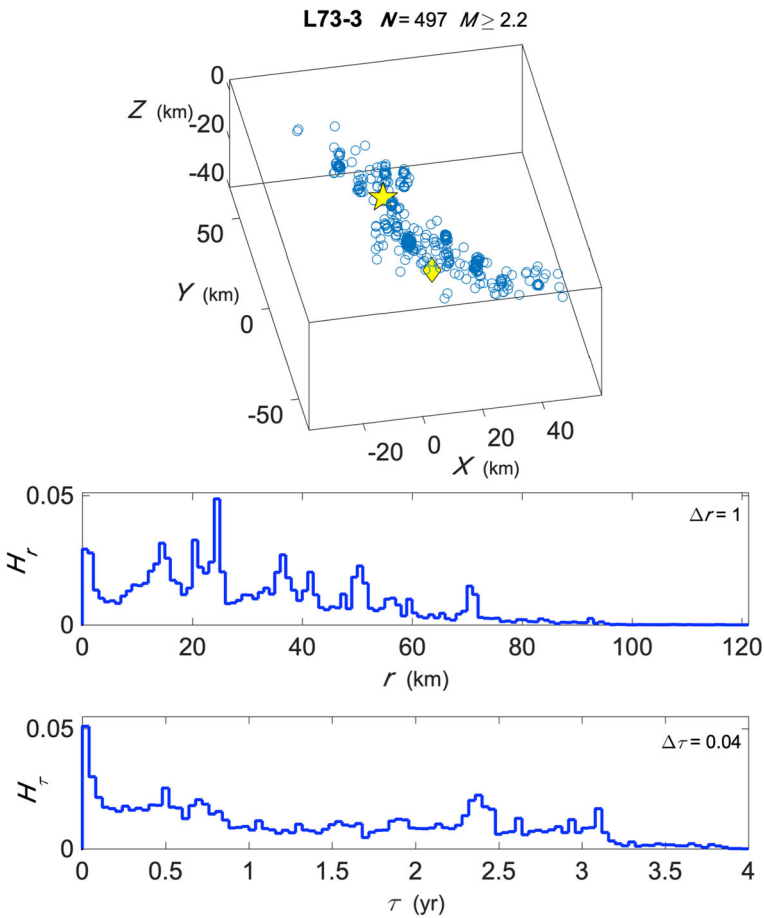
Fig. 11 Hypocenters of the L73 patch for the L73-3 time window (top). Distributions (histograms normalized by the total number of pairs N_p) for r and τ (bottom). The main and the Joshua Tree events are shown for comparison
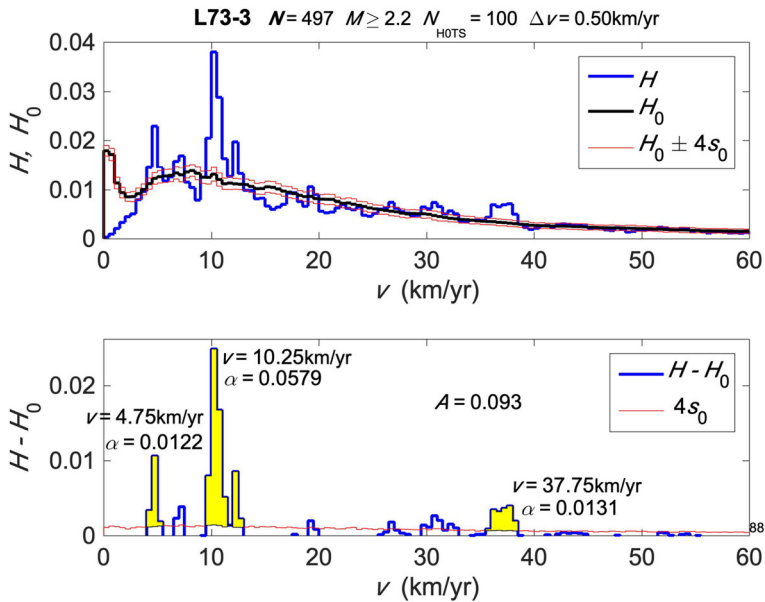
Fig. 12 Window 3 before L73. Velocity histograms; same conventions as in Fig. 6

NCs above $4s_0$ and α, respectively, are shown in the plot; the total NC above $4s_0$ is $A = 0.093$.

To show an example of event identification, the AVTP for velocities around those of the main peak of L73-3 is shown in Fig. 13, and two sample groups have been marked for analysis. Group 1 corresponds mainly to inter-cluster velocities, while group 2 is an example of intra-cluster velocities. After a group is chosen, the events contributing to it are identified and can be plotted (Fig. 14) to locate the site of the participating clusters and possibly relate them to some seismotectonic feature or to previous cluster activity.

Now, it remains to be seen whether significant peaks appear in other time windows. For reasons of space, the detailed analysis for each window will not be shown, but the time behavior of clustering can be clearly seen in Fig. 15, which shows $H - H_0$ for all windows, and the behavior of A with time can be compared with that before other earthquakes in Fig. 22.

Figure 15 clearly shows the largest A values for the third window before L73, L73-3; A values are consistently small for the windows 16 or more years before L73, as well as for the P window that serves as low-stress regime reference.

7.1 2010 $M_W = 7.2$ El Mayor-Cucapah Earthquake

The El Mayor-Cucapah $M_W = 7.2$ (EMC72) earthquake occurred on April 4, 2010 (2010.2573) at 115.2927°W, 32.2617°N.
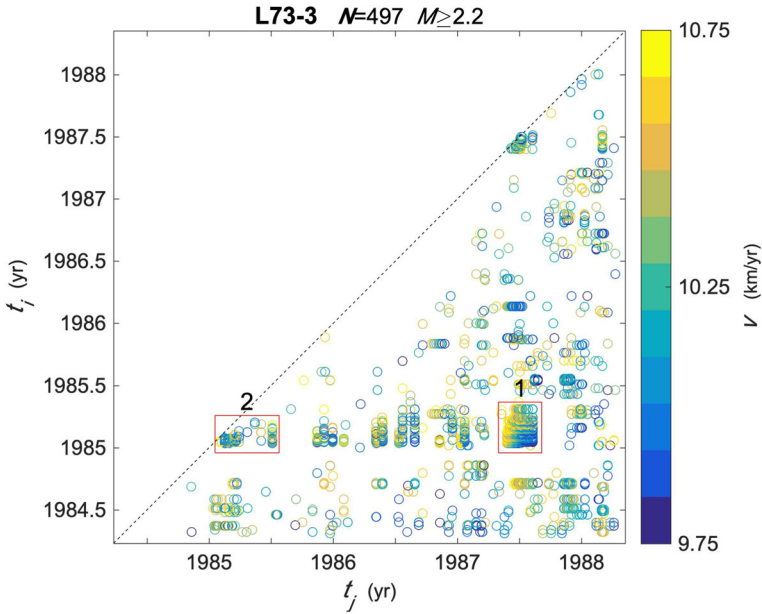
Fig. 13 AVTP AVs in the 9.75 to 10.75 v range in $t_i \otimes t_j$ space, colored according to the velocity color code at right. Example groups are shown as squares with an identification number on top
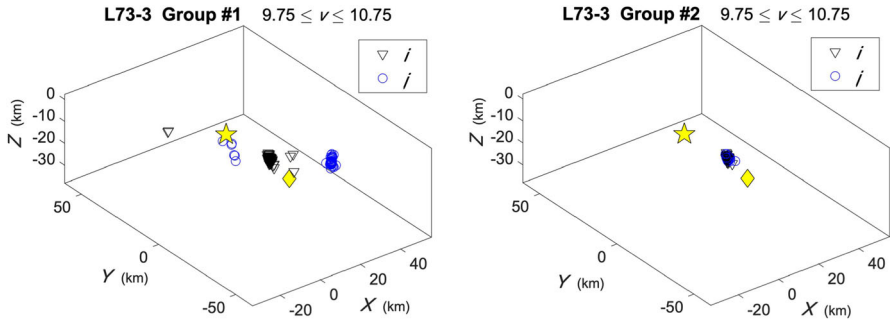
Fig. 14 Spatial location of the earthquakes constituting the groups identified in Fig. 13; group 1 (left) clearly shows two clusters plus a few external events, while group 2 (right) comprises mostly elements belonging to one cluster. The main event and Joshua Tree hypocenters are shown as a star and a diamond, respectively, for comparison

Figure 16 shows the epicentral space distribution of the EMC72 cluster and the time windows defined over the cumulative number of events graph; a star marks the position in space and time of the EMC72 earthquake. The first window ends right before the occurrence time of EMC72; all numbered windows are 4 years long, and their ending times are shifted backwards in time 2 years. The P low-stress reference window starts when aftershock activity has decreased to background level and is also 4 years long.
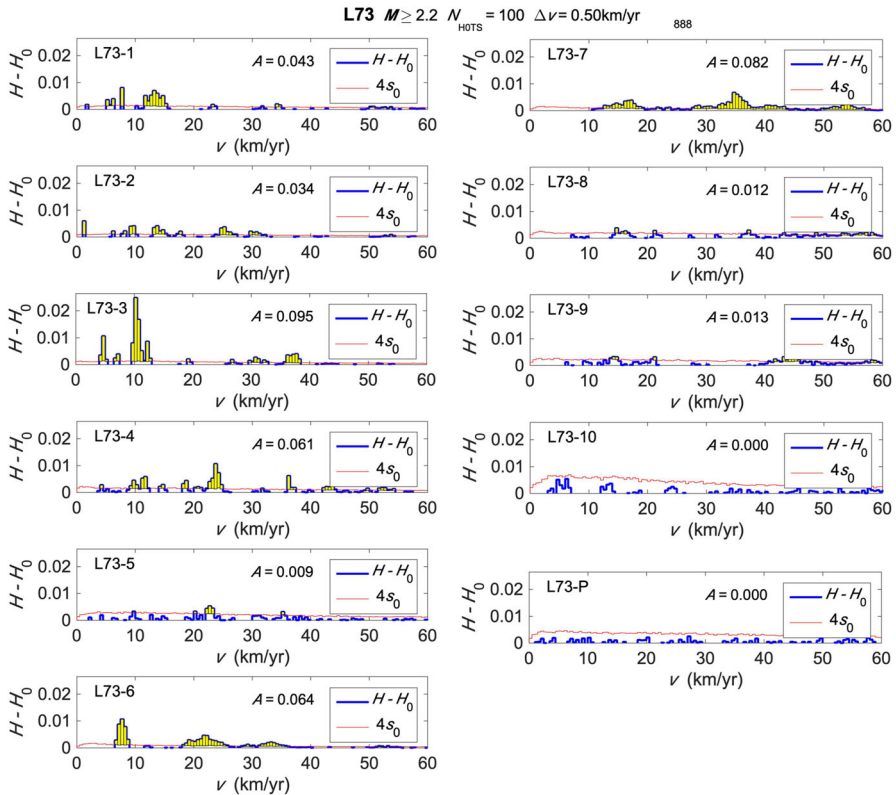
Fig. 15 L73 $H - H_0$ (thick blue line) and $4S_0$ distributions (thin red line) for the time windows indicated on each plot; classes with $H - H_0 > 4s_0$ (thin red line) have been shadowed, and the total fraction above $4s_0$ in these classes, A, is written on each plot

The $H - H_0$ and $4s_0$ curves for all windows are shown in Fig. 17 together with the corresponding A values. It is clear that for EMC72, the largest clustering occurred in window EMC72-1 just before the main event. Again, A values for times more than 10 years before EMC72 are either very small or zero, and the low-stress reference window EMC72-P has $A = 0.000$.

7.2 Hector Mine 1999 $M = 7.1$ Earthquake

The Hector Mine $M = 7.1$ earthquake (HM71) occurred on October 16, 1999 (1999.7901574) at 116.2687°W, 34.5957°N, and 20 km depth (Fig. 18, top). The cumulative number of events shown in the same figure indicates that the catalog does not have many events before HM71. On the other hand, there was no problem in selecting a window to explore the apparent velocities after the HM71 earthquake when seismicity was stabilized after most of the aftershocks; time windows are shown in Fig. 18 (bottom) and each is 4 years long.
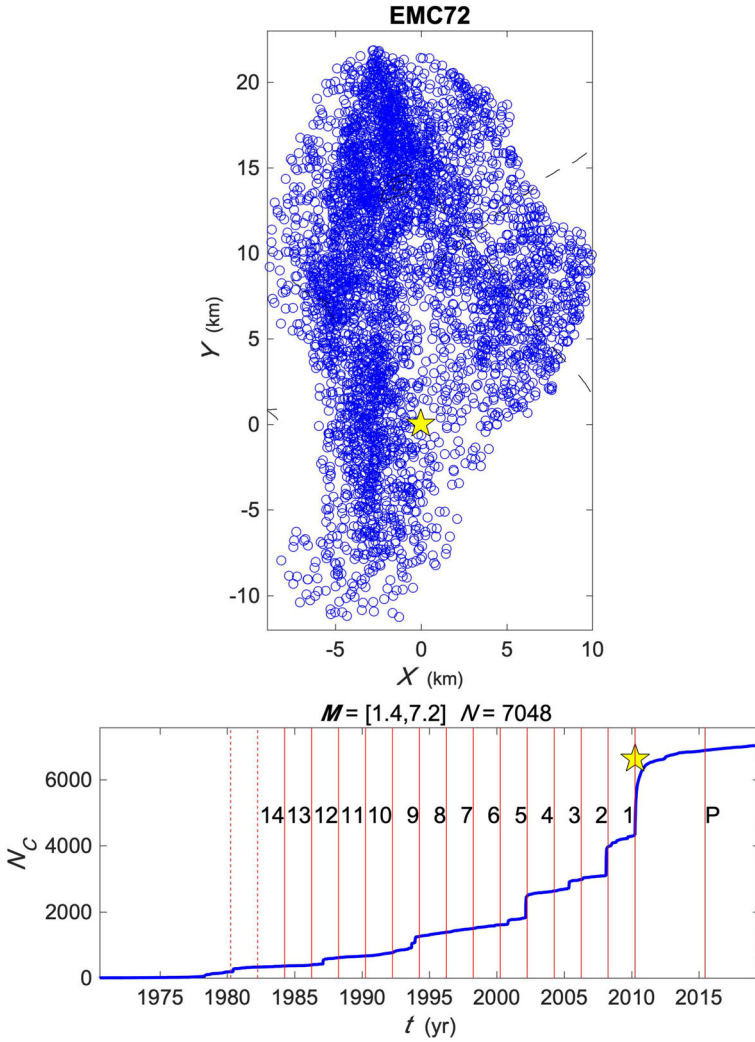
Fig. 16 Epicenter groups associated with the EMC72 earthquake (top), and cumulative number of earthquakes and time windows. Conventions are the same as in Fig. 10

The $H - H_0$ and $4s_0$ curves, together with the corresponding A values for all windows, are shown in Fig. 19. It is clear that for HM71, the largest clustering occurs in windows 3 and 2, a behavior closely resembling that of L73. Numbered windows more than ~12 years before HM71, as well as the low-stress reference window P, all show negligible A values.
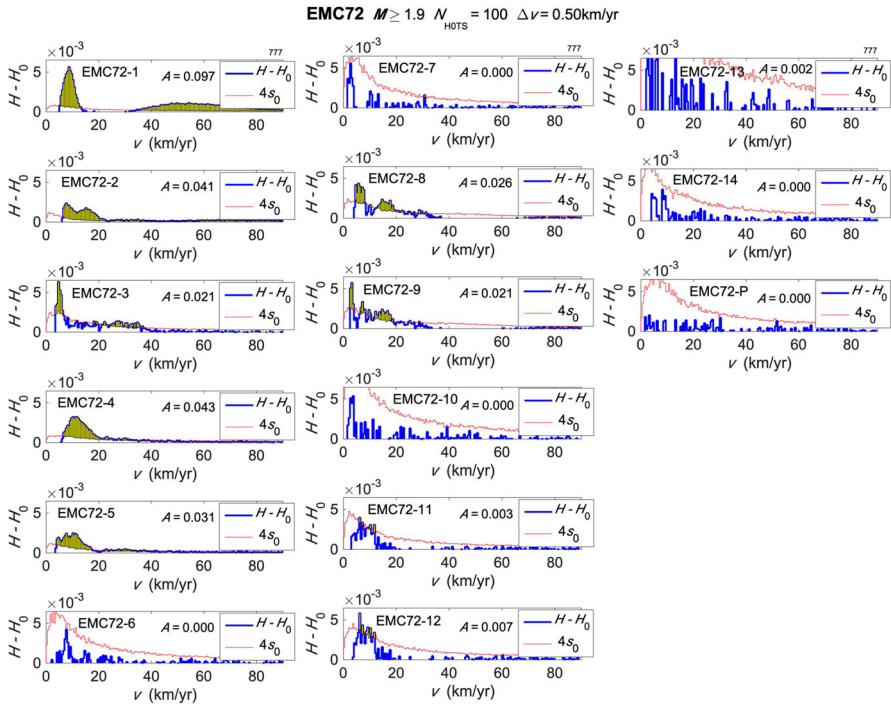
Fig. 17 EMC72 $H - H_0$ (thick blue line) and $4s_0$ (thin red line) distributions for the time windows indicated on each plot; classes with $H - H_0 > 4s_0$ have been shadowed, and the total fraction above $4s_0$ in these classes, A, is written on each plot

7.3 Ridgecrest 2019 $M_w = 7.1$ Earthquake

The July 6, 2019, Ridgecrest $M_w = 7.1$ earthquake occurred at $-117.599°$W and $35.770°$N at 8.00 km depth; this earthquake will be henceforth referred to as R71.

Figure 20 (top) shows the epicenter of R71 as a star, together with its associated patch of seismicity (circles), and the epicenter of the July 4, 2019, Searles Valley $M_w = 6.4$ earthquake that can be considered a foreshock to R71 (diamond). The figure also shows (bottom) the time windows used for the AV analysis; the first window ends right before the occurrence of the Searles Valley earthquake; each window spans 4 years, and ending times are shifted 2 years from the previous one. This being a recent earthquake, there was no time for a P window (Fig. 21).

7.4 Overall *A* versus Time for All Events

The *A* value versus time for all the studied earthquakes is summarized in Fig. 22. It is apparent that space–time clustering, as identified by the apparent velocity analysis *A* values, increases as time approaches that of the main earthquake and, with the exception of EMC72, decreases somewhat just before the earthquake.
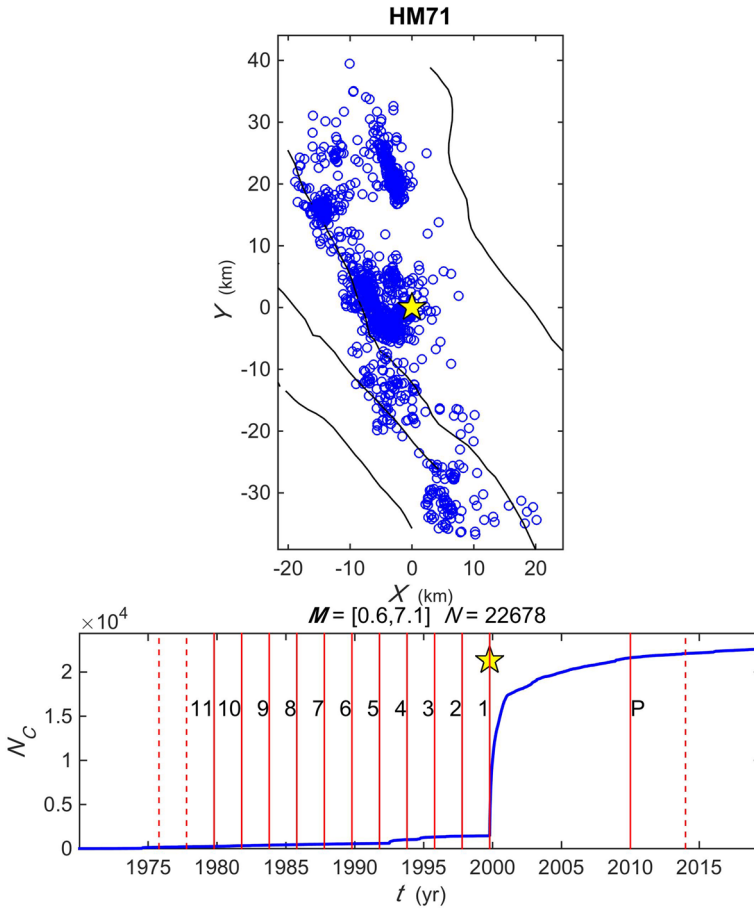
Fig. 18 Epicenter groups associated with the HM71 earthquake (top), and cumulative number of earthquakes and time windows. Conventions are the same as in Fig. 10

The high space–time clustering indicated by the high A values in the ~15 years before each large earthquake is interpreted as indicative of high-stress regimes, and the low values both long before the main earthquakes and after them in the P windows as indicative of low-stress regimes. For all earthquakes except EM72, clustering attains its largest value between 6 and 8 years before the main event, which occurs after clustering has decreased but not reached the background level. The EM72 main shock occurs right after the window with the highest value.

8 Discussion and Conclusions

The new method for space–time cluster identification and characterization using the occurrence of apparent velocities (AVs) presented in this paper is quite simple to
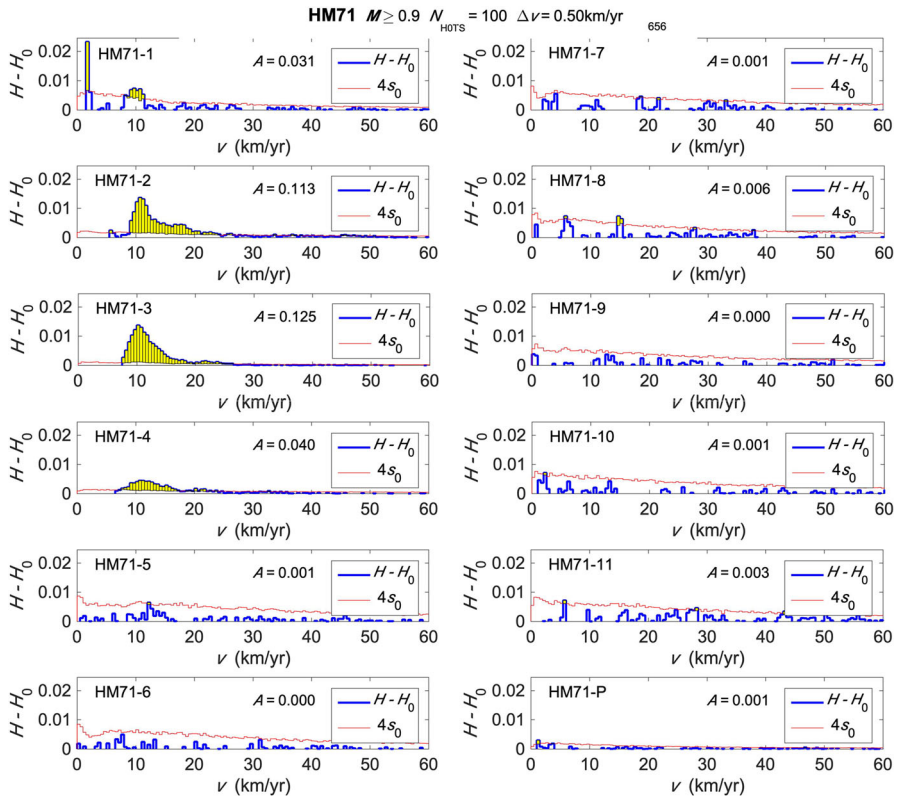
Fig. 19 HM71 $H - H_0$ (thick blue line) and $4S_0$ (thin red line) distributions for the time windows indicated on each plot; classes with $H - H_0 > 4s_0$ have been shadowed, and the total fraction above $4s_0$ in these classes, A, is written on each plot

implement and use and avoids the complications and a priori assumptions needed by most of the methods currently in use. The method is justified by the results from its application to seismicity before four large earthquakes in southern California and Baja California: large clustering in the 15 to 20 years before the mainshocks that reaches a maximum some 2 to 8 years before them, and no or negligible clustering long before the mainshocks or after them. When so desired, it is possible to locate the seismic clusters in time and space, so that the size and duration of the clusters are a result of the analysis and do not have to be estimated a priori.

Absolute errors in hypocentral locations using digital data from a well-distributed network can be of the order of hundreds of meters for epicenters and of kilometers for source depths; however, for pairs of events that are close in space and time, so that their waves follow similar paths to the seismic stations and their locations share the systematic errors from the velocity model and the location procedure, these errors will cancel when estimating the distance between each pair. Hence, one can expect events within each cluster to be well located relative to each other, so that intra-cluster velocities are not affected. Peaks due to inter-cluster velocities may appear at some
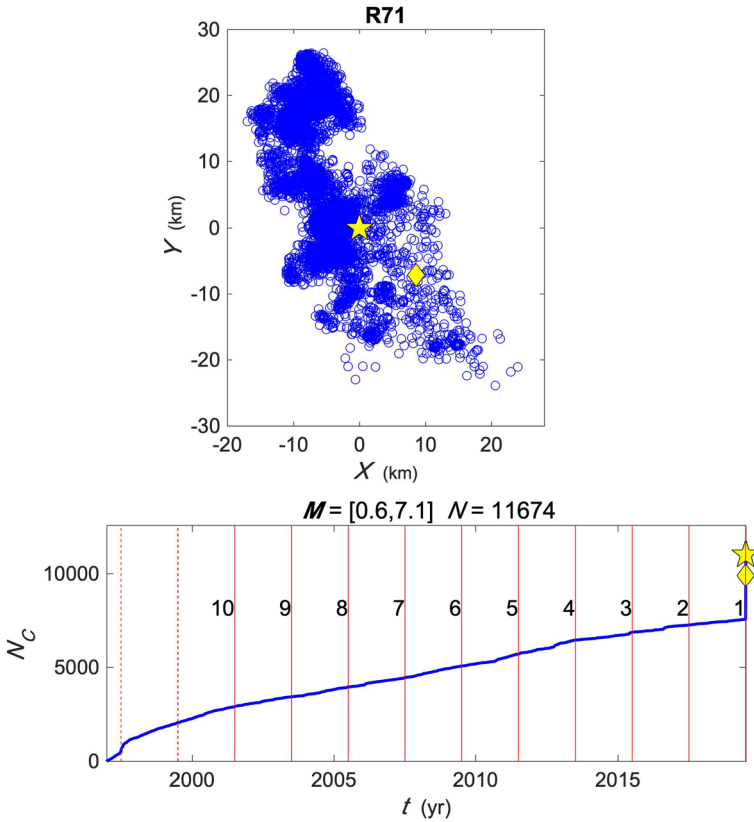
Fig. 20 Epicenter groups associated with the R71 earthquake (top), and cumulative number of earthquakes and time windows. Conventions are the same as in Fig. 10

velocity different from the one that would result from correct absolute locations, but the actual velocity at which peaks occur is immaterial, so this would not affect the peak appearances or the time–space cluster identification.

Is there a magnitude threshold limitation? Several windows from different earthquakes using different threshold magnitudes were tried (Reynoso 2019) and resulted in almost identical *A* values; hence, it is not necessary to have data complete to very small magnitudes and, coming back to the location limitations, the most poorly located events, the smallest ones, are not critical for clustering.
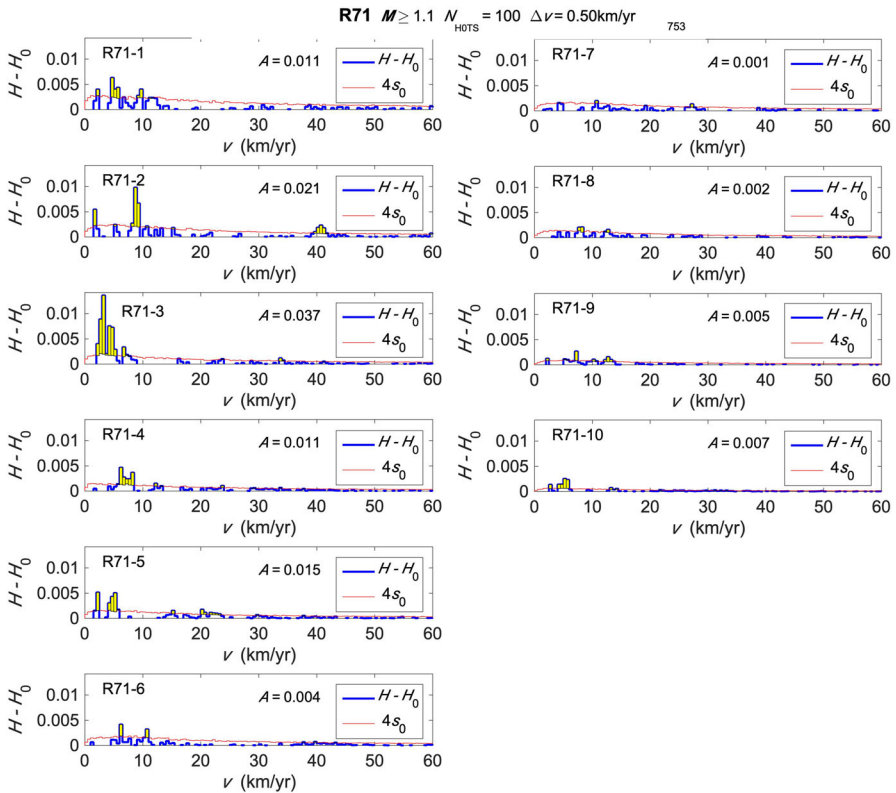
Fig. 21 R71 $H - H_0$ (thick blue line) and $4s_0$ (thin red line) distributions for the time windows indicated on each plot; classes with $H - H_0 > 4s_0$ have been shadowed, and the total fraction above $4s_0$ in these classes, A, is written on each plot

While full AVTP matrix analysis can be useful for locating active features, the authors think that the principal application of AV would be detecting precursory clustering, and this feature can be easily automated and implemented. The background seismicity in regions of interest can be sampled periodically, and if A values climb above a given level, determined for each region on the basis of analyses of seismicity before previous large earthquakes, the monitoring program can call attention to itself for seismologists to use this information for detailed analysis, search for foreshocks, and other activities that can contribute to reliable seismic hazard estimates.
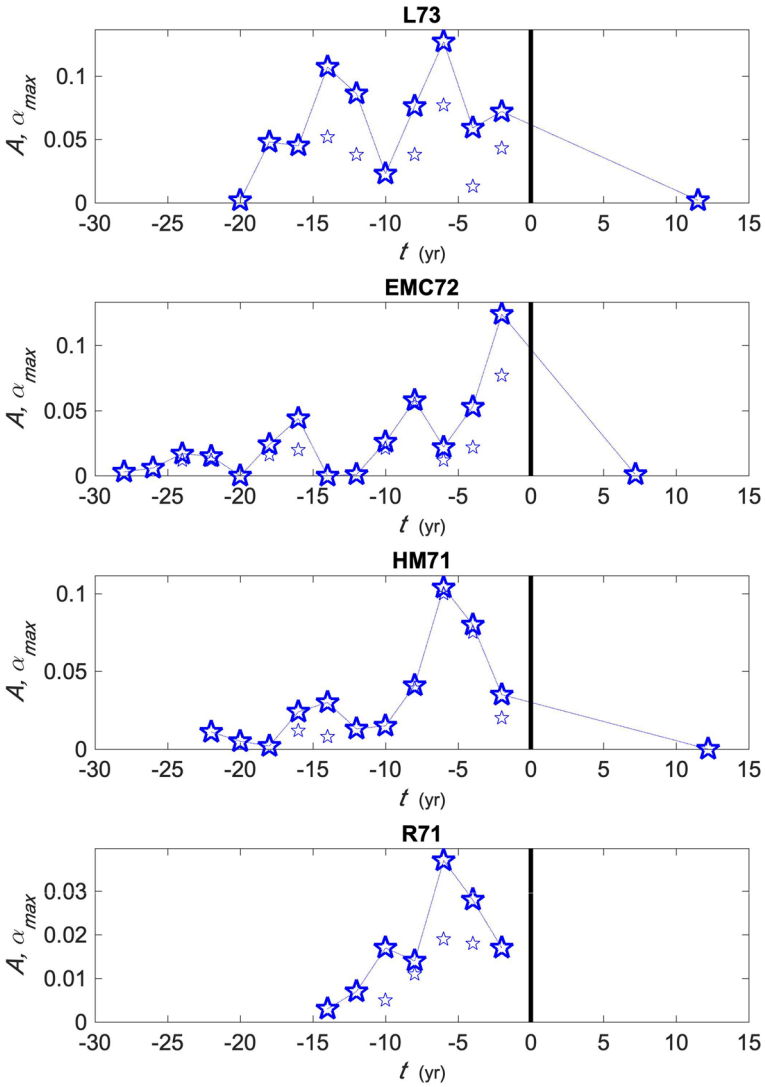
Fig. 22 *A* vs. time for all studied earthquakes. *A* is indicated by large stars, the largest single peak α, α_{max}, by small stars. Each symbol is located in time at the middle of the respective time window, and all times refer to the corresponding main event indicated by a thick vertical line

Declarations

Conflict of interest There are no financial or non-financial interests that are directly or indirectly related to the present work.

References

Adamaki AK, Roberts RG (2017) Precursory activity before larger events in Greece revealed by aggregated seismicity data. Pure Appl Geophys 174:1331–1343. https://doi.org/10.1007/s00024-017-1465-6

Aki K (1981) A probabilistic synthesis of precursory phenomena. In: Simpson DW, Richards PG (eds) Earthquake prediction: an international review, Maurice Ewing Series, vol 4. AGU, Washington, DC

Anderson JG (1982) Revised estimates for the probabilities of earthquakes following observation of unreliable precursors. Bull Seismol Soc Am 72:879–888

Chen Y, Liu J, Ge H (1999) Pattern characteristics of foreshock sequences. Pure Appl Geophys 155:395–408

Cicerone R, Ebel J, Britton J (2009) A systematic compilation of earthquake precursors. Tectonophysics 476:371–396. https://doi.org/10.1016/j.tecto.2009.06.008

Czecze B, Bondár I (2019) Hierarchical cluster analysis and multiple event relocation of seismic event clusters in Hungary between 2000 and 2016. J Seismolog 23(6):1313–1326

Dimitriu P, Scordilis E, Karacostas V (2000) Multifractal analysis of the Arnea, Greece seismicity with potential implications for earthquake prediction. Nat Hazards 21:277–295

Enescu B, Ito K (2001) Some premonitory phenomena of the 1995 Hyogo-Ken Nanbu (Kobe) earthquake: seismicity, b-value and fractal dimension. Tectonophys 338:297–314

Ester M, Kriegel H, Sander J, Xu X (1996) A density-based algorithm for discovering clusters in large spatial databases with noise. AAAI, KDD-96 96:226–231

Evison F (1999) On the existence of earthquake precursors. Ann Geophys 42:763–770

Frohlich C, Davis S (1990) Single-link cluster analysis as a method to evaluate spatial and temporal properties of earthquake catalogues. Geophys J Int 100:19–32

Geilikman M, Golubeva T, Pisarenko V (1990) Multifractal patterns of seismicity. Earth Planet Sci Lett 99:127–132

Goltz C (1997) Fractal and chaotic properties of earthquakes. In: Goltz C (ed) Fractal and chaotic properties of earthquakes, Lecture Notes in Earth Sciences, Vol 77. Springer, Berlin

Hauksson E (2011) Crustal geophysics and seismicity in southern California. Geophys J Int 186:82–98

Kanamori H (1981) The nature of seismicity patterns before large earthquakes. In: Simpson DW, Richards PG (eds) Earthquake prediction: an international review, Maurice Ewing Set, vol 4. AGU, Washington, DC

Lippiello E, Marzocchi W, de Arcangelis L, Godano C (2012) Spatial organization of foreshocks as a tool to forecast large earthquakes. Nature, Sci Rep 2:846

Main I, Al-Kindy F (2002) Entropy, energy, and proximity to criticality in global earthquake populations. Geophys Res Lett 29(7):1121. https://doi.org/10.1029/2001GL014078

Márquez V, Nava F, Reyes G (2012) Multifractality in seismicity spatial distributions: Significance and possible precursory applications as found for two cases in different tectonic environments. Pure Appl Geophys 169:2091–2105. https://doi.org/10.1007/s00024-012-0473-9

McGuire JJ, Boettcher MS, Jordan TH (2005) Foreshock sequences and short-term earthquake predictability on East Pacific Rise transform faults. Nature 434:457–461

Michas G, Sammonds P, Vallianatos F (2015) Dynamic multifractality in earthquake time series: Insights from the Corinth rift, Greece. Pure Appl Geophys 172:1909–1921. https://doi.org/10.1007/s00024-014-0875-y

Mignan A (2014) The debate on the prognostic value of earthquake foreshocks: a meta-analysis. Sci Rep 4:4099

Nanjo K, Hirata N, Obara K, Kasahara K (2012) Decade-scale decrease in b value prior to the M9-class 2011 Tohoku and 2004 Sumatra quakes. Geophys Res Lett 39:L20304. https://doi.org/10.1029/2012GL052997

Ogata Y, Utsu T, Katsura K (1995) Statistical features of foreshocks in comparison with other earthquake clusters. Geophys J Int 121:233–254

Parzen E (1960) Modern probability theory and its applications. Wiley, Tokyo

Rehman K, Burton PW, Weatherill GA (2014) K-means cluster analysis and seismicity partitioning for Pakistan. J Seismolog 18:401–419. https://doi.org/10.1007/s10950-013-9415-y

Reynoso H (2019) Velocidades aparentes y cúmulos espacio-temporales como precursores a grandes sismos. MSc Thesis, Centro de Investigación Científica y de Educación Superior de Ensenada, Baja California https://biblioteca.cicese.mx/catalogo/tesis/ficha.php?id=25583

Rikitake T (1976) Earthquake prediction (developments in solid earth geophysics). Elsevier, Amsterdam

Smith W (1986) Evidence for precursory changes in the frequency-magnitude b-value. Geophys J Int 86:815–838

Telesca L, Cuomo V, Lapenna V, Macchiato M (2001) Depth-dependent time-clustering behaviour in seismicity of southern California. Geophys Res Lett 28(22):4323–4326

Vidale J, Shearer P (2006) A survey of 71 earthquake bursts across southern California: exploring the role of pore fluid pressure fluctuations and aseismic slip as drivers. J Geophys Res Solid Earth 111(B5):B05312. https://doi.org/10.1029/2005JB004034

Wang J, Chen K, Leu P, Chang C (2016) Precursor times of abnormal b-values prior to mainshocks. J Seismol 20:905–919. https://doi.org/10.1007/s10950-016-9567-7

Weatherill G, Burton P (2009) Delineation of shallow seismic source zones using K-means cluster analysis, with application to the Aegean region. Geophys J Int 176(2):565–588

Wyss M (1991) Evaluation of proposed earthquake precursors. EOS Trans Am Geophys Union 72:411

Wyss M (1997) Second round of evaluations of proposed earthquake precursors. Pure Appl Geophys 149:3–16

Yang J, Cheng C, Song C, Shen S, Zhang T, Ning L (2019) Spatial-temporal distribution characteristics of global seismic clusters and associated spatial factors. Chin Geogra Sci 29(4):614–625

Zaliapin I, Ben-Zion Y (2013) Earthquake clusters in southern California I: identification and stability. J Geophys Res Solid Earth 118:2847–2864

Zaliapin I, Ben-Zion Y (2016) A global classification and characterization of earthquake clusters. Geophys J Int 207(1):608–634

Zaliapin I, Gabrielov A, Keilis-Borok V, Wong H (2008) Clustering analysis of seismicity and aftershock identification. Phys Rev Lett 101:018501

Zechar JD, Zhuang J (2010) Risk and return: Evaluating reverse tracing of precursors earthquake predictions. Geophys J Int 182:1319–1326. https://doi.org/10.1111/j.1365-246X.2010.04666